Sensors and Materials, Vol. 37, No. 7 (2025) 3317–3337
MYU Tokyo

S & M 4120

Enhancing Driver Fatigue Monitoring: A Hybrid Human–Machine Intelligence Framework with Adaptive Real-time Feedback

Tianjun Zhu,[1*†] Zizheng Zhu,[2†] Jianguo Liang,[1]
Pengcong Xian,[1] Zhuang Ouyang,[3] and Bin Li[4]

[1]Department of Mechanical and Automotive Engineering, Zhaoqing University, Zhaoqing 526021, China
[2]School of Automotive Studies, Tongji University, Shanghai 201804, China
[3]Guangdong Zhaoqing Institute of Quality Inspection & Metrology, Zhaoqing 526000, China
[4]Cummins Drivetrain and Braking Systems, 2135 W Maple Road, Troy, MI, 48098 USA

(Received March 31, 2025; accepted July 7, 2025)

Keywords: human–machine, hybrid BP neural network, driver fatigue detection

In this study, we sought to augment existing driver fatigue detection techniques, which are deficient in individual fatigue feature analysis, precision, and resilience. A novel driver fatigue monitoring intelligent system is introduced, employing human–machine hybrid enhancement. To address these limitations, a human–machine hybrid fatigue driving experimentation platform was designed using a hardware-in-the-loop system. This amalgamation delivers accurate fatigue level assessments. Subsequently, three preprocessing methods were compared for facial imaging and vehicular status data, developing a driver human–machine hybrid fatigue driving database. This comprehensive database includes facial images, steering wheel angle, and acceleration pedal data, aiding in detecting fatigue-induced behavioral shifts. Lastly, variance analysis was employed to quantify the significant difference levels of human–machine hybrid fatigue feature parameters across varying fatigue levels. On the basis of this analysis, a machine-learning-technique-based human–machine hybrid enhanced driver fatigue monitoring intelligent system was developed, achieving accuracies of 95.5%, 91.5%, 94.7%, and 95.0% in distinguishing four driver fatigue stages, namely, wakefulness, mild fatigue, fatigue, and severe fatigue, respectively. Our findings validate the efficacy of our proposed system in discerning driver fatigue levels and its potential to significantly improve transport system safety and efficiency.

1. Introduction

Driver fatigue is a significant threat to road safety. Recent data suggests an annual increase in accident rates attributable to fatigue. This alarming crisis has stimulated extensive research and development within the technological sector, focused on pioneering driver fatigue detection techniques, which are critical safeguards for transportation safety.

*Corresponding author: e-mail: zhutianjun@zqu.edu.cn
†Tianjiun Zhu and Zizheng Zhu are co-first authors.
https://doi.org/10.18494/SAM5670

ISSN 0914-4935
https://myukk.org/

Fatigue impacts driver performance, affecting concentration, reaction time, and judgment. Prolonged driving, inadequate rest, and physiological/psychological factors are the primary contributors. Fatigue driving can lead to severe consequences, jeopardizing the driver and potentially harming others.

The pursuit of effective fatigue detection technologies in road safety research has escalated. Advances have been marked by a surge of innovative concepts and experimental results, paving the way for advanced solutions capable of detecting driver fatigue and alerting drivers before it escalates. As these technologies become more prevalent and integrated into existing vehicle systems, they can serve as a potent deterrent against fatigue driving, ensuring a safer, more secure road network for all. Current fatigue detection technologies include the following:

1) Physiological signal detection: This strategy involves observing alterations in biological signs such as eyelid movements and pulse rate for gauging driver fatigue. Sensor information such as electroencephalography, electrooculography, electrocardiography, and electromyography are used for signal collection. Houshmand *et al.* devised a method based on electroencephalogram (EEG) alpha spindle waves for checking fatigue.(1) This method first uses continuous wavelet transform and Morlet function to identify EEG features, then uses convolutional neural network for the adaptive classification of EEG, and finally uses a self-learning method to determine early fatigue.(1) Jeong *et al.* presented a deep spatiotemporal convolutional bidirectional long short-term memory network model for fatigue detection.(2) This model employs BrainAmp equipment to gather EEG data from subjects, which is then preprocessed prior to detection. The fatigue level of the EEG signal is categorized into five stages and evaluated utilizing the Karolinska Sleepiness Scale (*KSS*) table, which indicates two psychological statuses and five fatigue levels.(2) Gromer *et al.* designed an electrocardiogram acquisition device that employs a sensor to gather heart rate variability data to detect driver fatigue.(3) Gao *et al.* proposed a novel approach for fuzzy feature integration and developed a comprehensive adaptive interpretable Takagi–Sugeno–Kang Fuzzy Classifier.(4) Zhong *et al.* introduced a two-stage framework that leverages graph neural networks and functional connectivity to identify mesoscopic regions in EEG signals, improving driver fatigue detection.(5) Guo *et al.* designed a Multi-modality Attention Network for driver fatigue detection, integrating frontal EEG, electrodermal activity, and photoplethysmography signals into a hybrid model.(6) Zhang *et al.* proposed a generative-AI-enhanced framework for multi-modal physiological signal analysis in intelligent transportation safety systems.(7) Although these methods exhibit high precision and durability, they require data collection equipment that may affect driver performance. Moreover, the costs of conducting the tests are substantial, the equipment size is considerable and inconvenient for transportation, and there are significant individual variations, limiting the application of this detection method primarily to laboratories or driving simulators, rendering it unsuitable for widespread adoption.
2) Facial feature detection for drivers: This method employs a camera to capture the driver's face, utilizing machine vision techniques such as facial key point localization and face detection to identify attributes such as eye gaze direction, blinking frequency (BF), eye aspect ratio, and Percentage of Eyelid Closure Over Time (PERCLOS). Extracted features

include head movement, head rotation angle, and mouth aspect ratio, all detected using advanced algorithms. Carnegie Mellon University has conducted consistent testing to determine the PERCLOS parameter that measures fatigue. PERCLOS has three standards: EM, P70, and P80. Among these, P80 is deemed the superior standard for assessing human fatigue and is frequently used by researchers to evaluate a driver's mental state.[8] Anitha *et al.* proposed a yawn detection system that utilizes the upper and lower parts of the face. Mouth features from the lower face are extracted, and binary images are used to detect yawning and assess the driver's condition. [9] The fatigue detection method that utilizes driver facial characteristics offers several advantages, including affordability, non-intrusive nature, ease of implementation, minimal equipment, seamless integration, reasonable precision, and immediate monitoring. However, challenges arise when the driver's head is excessively tilted, they wear sunglasses, or the ambient lighting is inadequate, leading to unidentifiable occurrences.

3) Intelligent sensors: This method utilizes onboard sensors that collect data on vehicle acceleration, steering wheel rotation angle, and so forth, to analyze and determine the driver's fatigue level.[10] This approach provides real-time monitoring, accuracy, and portability. McDonald *et al.* input data such as steering angle, pedal positions, vehicle speed, and acceleration into a dynamic Bayesian network algorithm to detect driver fatigue.[11] Li *et al.* utilized the approximate entropy of the steering wheel angle sequence to select input data and extracted fatigue-related features using LSTM units.[12] They also used the information gain method to identify correlations between potential features and fatigue to obtain the most effective representation of fatigue features. Li *et al.* proposed a method to detect driver fatigue by measuring steering wheel grip strength.[13] This method determines the driver's mental state by analyzing the discrepancy between the steering wheel grip strength and the standard deviation of grip strength when the driver operates the vehicle. Zhu *et al.* proposed a multilayer adaptive driver fatigue monitoring model on the basis of the steering wheel signals obtained from 25 participants in a driving simulator.[14]

Fatigue exhibited by drivers manifests in their vehicle's behavior, which includes speed, acceleration, yaw angle, and lane deviation. These distinctive features are captured via sensors and scrutinized to detect driver consciousness. Pomerleau engineered an adaptable lateral position handler system. This system utilizes road image analysis through template matching and testing strategies, estimating vehicle deviation displacement, and subsequently determining driver state.[15] Cai *et al.* utilized the controller area network bus to record vehicle behavior data, extracting 18 features such as speed, acceleration, and pedal usage. The Pearson correlation coefficient is employed to assess feature correlation with fatigue, and four algorithms are applied to detect driver fatigue.[16]

Driver-status-focused fatigue detection methods offer advantages including accessible data collection, affordability, compact equipment, transportation convenience, and comparable precision. They hold potential in the market and are easily deployed and operated. Nevertheless, they may become vulnerable to road conditions, driver proficiency, and driving habits.

The main contribution of this study is that multiple strategies for fatigue driving detection are proposed, despite some challenges. For example, by utilizing facial driver video capture

technology, recognition accuracy may be reduced due to differences in lighting intensity. To improve the accuracy and reliability of fatigue detection methods and enhance their overall generalization ability, it is urgent to propose a new type of fatigue detection method. In this study, we utilized a human–machine hybrid enhanced driver fatigue monitoring system based on deep learning. The driver fatigue detection model based on multi-feature fusion proposed in this paper effectively solves the limitations of single data source fatigue detection, providing theoretical and technical support for subsequent fatigue detection model research.

This paper's structure is as follows:

In Sect. 2, we have established a complex hardware-in-the-loop system platform for driver fatigue driving detection. A comprehensive simulation experiment design was specifically formulated. Nine expert drivers were recruited for fatigue driving experiments on the platform. Comprehensive driving status and facial features were meticulously collected from these drivers at various fatigue stages.

In Sect. 3, we describe the data processing methods used in this article. Local histogram equalization (LHE), fast automatic color equalization, and adaptive contrast enhancement (ACE) are employed to balance the image illumination and improve the image recognition accuracy. Driving status data preprocessing involves the use of Carmaker's control software for exporting data for further analysis, excluding turning and lane changing data. After preprocessing, data is segmented on the basis of the driver's *KSS* score and four-level fatigue judgment method to establish a fatigue sample database.

In Sect. 4, we identified the features for fatigue driving assessment, including vehicle information and driver facial features.

In Sect. 5, a human–machine hybrid enhanced driver fatigue monitoring system employing the back propagation neural network was implemented.

In Sect. 6, the system was developed using machine learning techniques (deep learning) within a Pycharm Integrated Development Environment. The process involved the random selection of training and testing sample sets for system training and validation.

2. Driver Fatigue Driving Platform

Given the significant safety risks in authentic road fatigue driving experiments, ensuring driver and staff safety or validating driving investigation accuracy is unattainable. Existing fatigue detection research primarily utilizes driving simulators as substitutes.

2.1 Experimental platform

In this study, we utilized a bespoke simulated driving platform, a hardware-in-the-loop system driving simulator, and relevant software (incorporated by Carmaker and Matlab/Simulink).

The fatigue driving experimental platform incorporates a driving simulator, a National Instruments real-time system, and an HD camera, coupled with pertinent software (including Carmaker and Matlab/Simulink software). The driving simulator has three components: driving

platform, 6-DOF simulation platform, and visual display system. The specific driver fatigue driving platform is shown in Fig. 1.

2.2 Experimental drivers

Nine drivers (7 males and 2 females) aged between 22 and 28 and with driver's licenses and extensive driving experience participated in the fatigue driving tests. All drivers' driving states are shown in Figure 2. The testing personnel maintained optimal health conditions to minimize variations in outcome. Participants refrained from alcohol consumption and refreshing beverages the day before the test, ensuring a minimum of eight hours of sleep. To ensure the confidentiality of experimental data, protect the privacy of experimenters, and ensure the integrity of data, all drivers must sign an informed consent form before conducting the experimental testing, and they need to understand how their experimental data will be used.

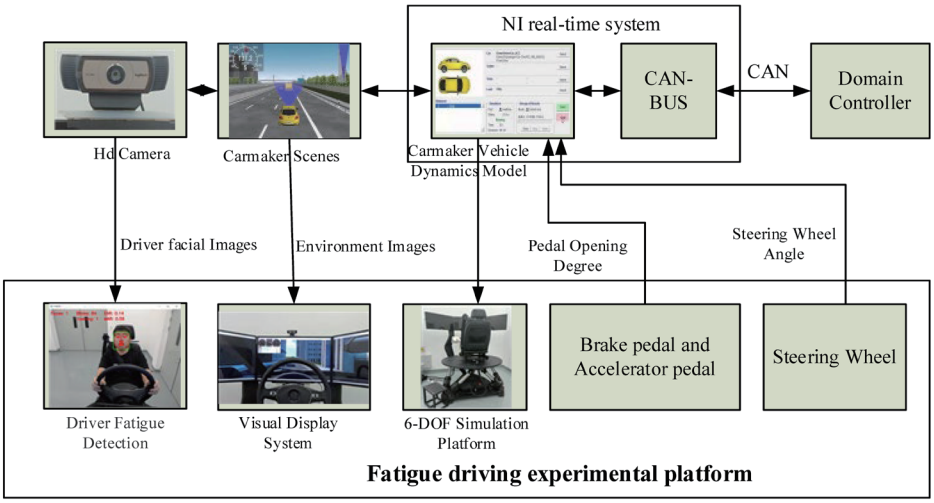

Fig. 1. (Color online) Fatigue driving experimental platform.

Fig. 2. (Color online) Driver driving scenes under different ambient lighting conditions.

The objective of this study was to gather driving status data and facial characteristics of drivers in varying fatigue states, encompassing waking, mild fatigue, fatigue, and severe fatigue. Considering drivers' routine, fatigue may occur around 14:00 PM or 1:00 AM. Hence, fatigue driving experiments were conducted from 13:00 to 15:00 PM and 1:00 to 3:00 AM, allowing a comprehensive recording of drivers' fatigue states and facilitating future research.

2.3 Road simulation scene design

To ensure that the experimental data is closer to real driving situations, driver fatigue driving experiments were conducted in different single road environments and under different environmental lighting conditions to further expand the diversity of the experimental dataset. On the basis of the above environment that causes fatigue for drivers, different road environments were designed. In this study, we created four driving scenarios, namely, driving on highways during the day, driving on urban expressways during the day, driving on highways at night, and driving on urban expressways at night. The specific road simulation scenes are shown in Table 1.

If there is no traffic flow and various driving vehicles in the simulated road environment, there may be significant differences between the simulated road and the actual road conditions, which may lead to driver distraction and relaxation. To get closer to the actual traffic situation, the simulated road detailed in this article incorporates synchronized traffic flow, including both opposing and approaching vehicles. This aligns better with the actual road environment, ensuring a more realistic data collection. This study's data collection environment mainly comprises two traffic scenarios, highways and urban expressways, simulating the Zhaoqing City to Guangzhou highway road with a total distance of 300 km, as illustrated in Fig. 3(a), and the Duanzhou District urban expressway road with a total distance of 100 km, as depicted in Fig. 3(b). The entire expressway features six lanes in each direction, with a standard maximum width of 3.75 m per lane. Throughout the journey, there are four lanes in each direction, each measuring 3 m wide.

3. Data Preprocessing Methods

When the driver accelerates, variations in cab or outdoor light levels result in fluctuations in camera video image intensity, blurring, and other nuisances. Such inconsistent and blurred illumination interferes with fatigue feature parameter identification, impacting detection precision.

Table 1
Road simulation scenes.

Scenario	Scenario abbreviation	Scenario overview
Scenario 1	DH	day, driving on highways
Scenario 2	DUE	day, driving on urban expressways
Scenario 3	NH	night, driving on highways
Scenario 4	NUE	night, driving on urban expressways

(a) (b)

Fig. 3. (Color online) Road environments: highways and urban expressways. (a) Highway and (b) urban expressway routes

We explored three strategies, namely, LHE, fast automatic color balancing (ACB), and ACE, to attain illumination equalization on captured images, thereby enhancing clarity.

3.1 LHE

Histogram equalization aims at normalizing the original image's histogram to the new distribution through its cumulative distribution function, hence homogenizing the gray scale level and enhancing image illumination.[17] Image histogram equalization is solved through a discrete form of cumulative distribution function, and the mapping method during the histogram equalization process is performed using Eq. (1).

$$S_k = \sum_{j=0}^{k} \frac{n_j}{N}, \ k = 0,1,2,\cdots,L = 1 \tag{1}$$

Here, S_k represents the value of the current gray level after being mapped by the cumulative distribution function, N represents the total gray level of pixels in an image, n_j represents the number of pixels in grayscale level, and L represents the total number of gray levels in the image.

The impact of illumination on images can be divided into two types: global and local. The global impact indicates that the overall illumination of the image is either too high or too low. In this case, it is necessary to perform equalization processing on the entire image, but the computational cost is relatively high. The illumination has a significant impact on the driver's facial image, so only local equalization processing is needed for the driver's facial image, which has high processing efficiency and good accuracy.

The steps of LHE are as follows:

(1) Scan each pixel of the original grayscale image sequentially and calculate the grayscale histogram of the image.
(2) Calculate the cumulative distribution function of the grayscale histogram.
(3) Obtain the mapping relationship between input and output based on the cumulative distribution function and histogram equalization principle.
(4) Obtain the results based on the mapping relationship and perform image transformation.

Figure 4 shows the impact of LHE on video image processing under different lighting conditions. The upper image shows the processing result of the driver's facial image using the LHE method under good lighting conditions. The lower image shows the processing result of the driver's facial image using the LHE method under night or poor lighting conditions. It can be clearly seen that the LHE method can effectively process the driver's facial image under good lighting conditions. However, in nighttime or poor lighting environments, the LCE method may not have a very clear effect on the processing of driver facial images.

3.2 Fast ACB

Narendra *et al.* developed a method based on Retinex theory for color equalization.[18] This technique utilizes the spatial phase relation of color and brightness for adapting local image patches, regulating both image brightness and color, and altering contrast.

Fast ACB mainly adjusts the color of images to achieve color difference correction, which can be represented by Eq. (2).

$$R_c(p) = \sum_{j \in Subset,\, j \neq p} \frac{r\left(I_c(p) - I_c(j)\right)}{d(p,j)} \tag{2}$$

Here, R_c is an intermediate result of image processing, I_c is the original input image, c represents the color channel, $I_c(p) - I_c(j)$ represents the difference in brightness between pixel points p and j, $d(p, j)$ is the distance function between pixel points p and j, and r(*) represents the relative brightness function, mainly used to explain the difference in relative brightness between a point and its nearby points. r(*) is shown in Eq. (3) below.

Fig. 4. (Color online) Comparison before and after LHE.

$$r(x)=\begin{cases} 1 & x<-1 \\ \dfrac{x}{T} & -1\le x\le T \\ -1 & x>T \end{cases} \tag{3}$$

Here, the parameter T is the saturation critical value, which can be adjusted reasonably according to actual needs to obtain the expected value.

The fast automatic color balance algorithm is applied to a single color channel, and for color images, each color channel needs to be processed separately. Figure 5 shows the effect after ACB processing.

As shown in Fig. 5, the ACB algorithm improves the overall visual effect of the image by calculating the local contrast of each pixel and enhancing it. The ACB algorithm is suitable for image processing in low-contrast (poor lighting) environments. Therefore, compared with the LHE algorithm, it has better performance in processing the facial images of night drivers.

3.3 ACE

ACE divides an image into two components: the low-frequency and high-frequency sections. The former is attained through low-pass filtering, whereas the latter arises by subtracting the filtered result from the original image. ACE mainly achieves image enhancement by changing the gain coefficient of the high-frequency part.

Owing to the fact that an image is composed of numerous pixels, $M(i, j)$ is represented as a region centered around a point (i, j) with a window size of $[(2n + 1) \times (2m + 1)]$. The local mean and variance can be expressed using Eqs. (4) and (5), respectively.

$$M(i,j)=\frac{1}{(2n+1)(2m+1)}\sum_{k=i-n}^{i+n}\sum_{l=j-m}^{j+m} f(k,l) \tag{4}$$

Fig. 5. (Color online) Comparison before and after ACB processing.

$$\sigma^2(i,j) = \frac{1}{(2n+1)(2m+1)} \sum_{k=i-n}^{i+n} \sum_{l=j-m}^{j+m} \left[f(k,l) - M(i,j) \right]^2 \tag{5}$$

Here, $f(k, l)$ represents the pixel value when the coordinate is (k, l), $M(i, j)$ represents the local mean, and $\sigma^2(i, j)$ represents the local variance. Gain convolution is applied to the high-frequency part.

$$I(i,j) = M(i,j) + G\left[f(i,j) - M(i,j) \right] \tag{6}$$

$$G = \alpha \frac{M}{\sigma(i,j)} \tag{7}$$

Here, $I(i, j)$ denotes pixel values after enhancement processing, G is gain value, and α is coefficient parameters, $0 < \alpha < 1$. Usually, G is greater than 1, so using $G[f(i, j) - M(i, j)]$ can enlarge the high-frequency part of the image, thereby enhancing the processed image. Figure 6 shows the effect before and after ACE.

As shown in Fig. 6, the ACE algorithm enhances the high-frequency part of the image (i.e., the driver's facial area) by analyzing local regions of the image, thereby improving the contrast of the image. Through the ACE algorithm, the contrast of the driver's facial image can be significantly improved, which can enhance the details and visual effects of the image.

By comparing the images before and after processing using the three different lighting equalization methods mentioned above, it can be seen that LHE and fast automatic color balance methods have good processing effects on images with dark lighting, but have poor processing effects on images with bright lighting. The ACE method not only has good processing effects on images with dark light but also on images with bright light. Therefore, we adopted an ACE method to balance the illumination of collected driver facial images.

Fig. 6. (Color online) Comparison before and after ACE.

4. Feature Selection for Fatigue Driving Assessment

4.1 Subjective driving fatigue evaluation

The subjective fatigue status of 10 subjects (numbers for A–J) in the driving experiment designed in this study was investigated by questionnaire. To ensure the authority and accuracy of the fatigue level of the subjects, the internationally recognized *KSS* was used to score the fatigue level.

In this study, we used the criteria for determining level 4 fatigue and the *KSS* sleep scale to classify drivers from wakefulness to severe fatigue into four levels: awake, mild fatigue, fatigue, and severe fatigue. The four level fatigue assessment method can more clearly analyze the process of drivers transitioning from a conscious state to a severe fatigue state. Research shows the following: $KSS \leq 3$ indicates that the driver is at the awake level, $3 < KSS \leq 5$ indicates that the driver is at a slight fatigue level, $5 < KSS \leq 7$ indicates that the driver is at a fatigue level, and $KSS > 7$ indicates that the driver is at a severe fatigue level.[19]

4.2 Fatigue performance analysis of driving data

We compiled driving status data from a six-degree-of-freedom driving simulator, encompassing steering wheel angle and accelerator pedal opening and closing. Turning and lane-changing maneuvers were excluded from the collected data as extreme steering actions skew experimental precision. Given the IPG-generated erg format in Carmaker software, the IPG Control data processing software was employed for data management. This tool permits both real-time observation of simulated road vehicle states and postprocessing of simulation data, exportable in diverse formats for further data analysis software treatment.

The analysis considered steering wheel angle data from the vehicle lateral control and throttle pedal opening data from the vehicle longitudinal control. It evaluated driver's driving conditions, investigated driver state shifts across varying fatigue thresholds, and chose suitable driving state parameters to assist in detecting fatigue driving.

4.2.1 Steering wheel angle

The driver must actively monitor the environment and road conditions to ensure safety during driving, particularly when managing the steering wheel and adjusting accordingly as fatigue sets in over extended periods. The fluctuation in steering wheel angle can serve as an indicator of the driver's fatigue level.

Studies indicate that when drivers navigate in a straight path, the amplitude of steering wheel angle, the frequency of abrupt steering wheel changes, and the standard deviation of steering wheel angle all progressively increase over time. Therefore, we used the Absolute Mean of Steering Wheel (*AMSW*) angle and the Standard Deviation of Steering Wheel (*SDSW*) angle as indicators for driver fatigue assessment.

Neglecting the steering wheel's direction of rotation, we focused solely on magnitude. Thus, *AMSW* symbolizes the mean, determined by absolute steering wheel angle, which equates to

$$AMSW = \frac{1}{N}\sum_{i=1}^{N}\left|SW_i\right|. \tag{8}$$

In the above equation, N is the number of sampling points, and SW_i is the steering wheel angle.

The calculation formula for the steering wheel angle's standard deviation *SDSW* is

$$SDSW = \sqrt{\frac{1}{N-1}\sum_{i=1}^{N}\left(SW_i - SW_m\right)^2}. \tag{9}$$

The above equation defines $SW_m = \frac{1}{N}\sum_{i=i}^{N} SW_i$ as the average steering wheel angle.

Figures 7 and 8 illustrate the evolution of the steering wheel angle's mean and standard deviation during simulated driving, respectively. These graphs reveal an increase in the absolute mean and standard deviation of the steering wheel angle throughout the driving phase.

Ten driver fatigue samples were chosen for analysis, encompassing levels of awake, mild, fatigue, and severe fatigue, for 5, 10, and 15 s intervals. The data was analyzed through variance measurement to assess differences in mean steering wheel angle and standard deviation across fatigue levels. The significance level is the probability of making errors when estimating the population parameters falling within a certain interval, represented by α. Under the condition of determining significance level α equal to 0.05, the findings are presented in Table 2.

As shown in Table 2, when the selected time window equals 10 s, both *P*-values for *AMSW* and *SDSW* fall below 0.05, implying that *AMSW* and *SDSW* are suitable indicators for evaluating driver fatigue, with their *F*-values reaching a peak. Hence, the optimal extraction time boundary for these parameters is 10 s.

4.2.2. Throttle pedal opening

The throttle pedal opening is a key indicator of a driver's mental state. When the driver is energetic or has strong alertness, the driver's control accuracy of the throttle pedal is high, and

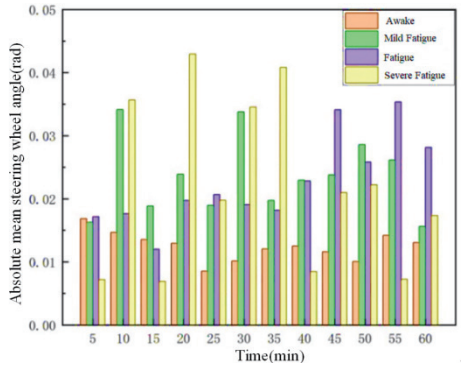

Fig. 7. (Color online) *AMSW* angle over time.

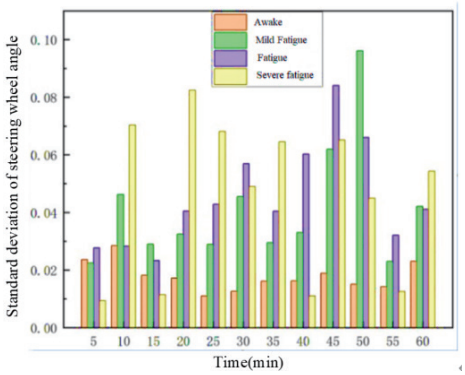

Fig. 8. (Color online) *SDSW* angle over time.

Table 2
Analysis of the absolute mean and standard deviation of the steering wheel angle.

Parameters	Time window (s)	Awake		Mild fatigue		Fatigue		Severe fatigue		*F* value	*P* value
		Absolute mean	Standard deviation	Absolute mean	Standard deviation	Absolute mean	Standard deviation	Absolute mean	Standard deviation		
AMSW	5	0.015	0.002	0.020	0.007	0.017	0.003	0.023	0.016	1.017	0.073
	10	0.011	0.002	0.021	0.006	0.020	0.002	0.026	0.013	1.533	0.038
	15	0.012	0.002	0.022	0.005	0.025	0.004	0.031	0.006	1.061	0.093
SDSW	5	0.022	0.005	0.033	0.009	0.030	0.006	0.043	0.033	0.774	0.062
	10	0.014	0.002	0.034	0.007	0.050	0.009	0.048	0.023	1.349	0.012
	15	0.018	0.004	0.056	0.027	0.056	0.021	0.056	0.020	0.836	0.079

the vehicle can maintain stable and efficient driving in the lane. When the driver's mental state is poor or there are fatigue symptoms, the stability of the throttle pedal control decreases, causing the vehicle to move fast and slow in the lane. Therefore, the driver's control of the throttle pedal opening can reflect the driver's mental state. Therefore, in this study, we selected the throttle pedal opening to analyze driver fatigue.

We employed Average Throttle Pedal Opening (*ATPO*) and Standard Deviation of Throttle Pedal Opening (*SDTPO*) as key indicators to detect driver fatigue. *ATPO* is expressed as

$$ATPO = \frac{1}{N}\sum_{i=1}^{N} TPO_i \,. \tag{10}$$

In the above equation, N is the number of sampling points for the sample, and TPO_i is the throttle pedal opening. The calculation formula for the standard deviation *SDTPO* of throttle pedal opening is

$$SDTPO = \sqrt{\frac{1}{N-1}\sum_{i=1}^{N}\left(TPO_i - TPO_m\right)^2} \,. \tag{11}$$

In the above equation, $TPO_m = \frac{1}{N}\sum_{i=1}^{N} TPO_i$ represents the overall average of throttle pedal opening.

Figures 9 and 10 depict the evolution of the average and standard deviation of driver throttle pedal opening levels throughout simulated driving, respectively. The data indicate that as driving duration extends, both average and standard deviation diminish. As fatigue escalates, the driver's longitudinal vehicle control diminishes, leading to compromised accelerator pedal precision.

We randomly selected 10 samples from each of the four fatigue levels, calculating the mean and standard deviation of the accelerator pedal position across three time frames of 60, 120, and 180 s. The variance analysis verifies levels. The comparison of mean and standard deviation values for different fatigue levels at $\alpha = 0.05$ is shown in Table 3.

The data indicate notable disparities in the mean and *SDTPO* across various fatigue levels. Assigning a 120-s window for these values demonstrated significant variations across fatigue

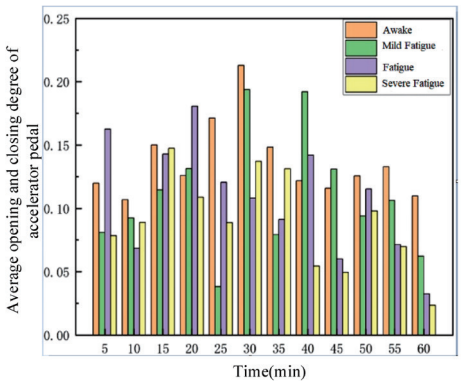

Fig. 9. (Color online) *ATPO* over time..

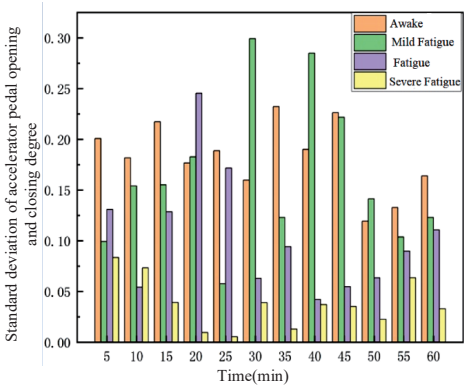

Fig. 10. (Color online) *SDTPO* over time.

Table 3
Analysis of the absolute mean and standard deviation of the steering wheel angle.

Parameters	Time window (s)	Awake		Mild fatigue		Fatigue		Severe fatigue		*F* value	*P* value
		Absolute mean	Standard deviation	Absolute mean	Standard deviation	Absolute mean	Standard deviation	Absolute mean	Standard deviation		
ATPO	60	0.122	0.194	0.126	0.148	0.106	0.114	0.108	0.071	0.434	0.045
	120	0.141	0.203	0.139	0.202	0.116	0.176	0.104	0.031	0.759	0.043
	180	0.120	0.181	0.099	0.221	0.103	0.066	0.138	0.049	0.756	0.049
SDTPO	60	0.112	0.201	0.058	0.099	0.048	0.131	0.033	0.083	6.336	0.047
	120	0.118	0.182	0.081	0.154	0.027	0.073	0.015	0.054	13.750	0.021
	180	0.125	0.217	0.055	0.155	0.049	0.129	0.012	0.039	9.608	0.025

levels ($F = 0.759$, $P = 0.043 < 0.05$; $F = 13.750$, $P = 0.021 < 0.05$). Thus, the average and variance of accelerator pedal movement can serve as fatigue indicators for driver fatigue recognition. The optimal time window chosen is 120 s.

4.3 Fatigue analysis on facial features

Studies indicate that variations in the eyes manifest most prominently during fatigue, followed by modifications in the mouth. Fatigue detection within facial features primarily employs eye and mouth characteristics.

However, facial feature fatigue detection necessitates specific collection equipment and environment conditions. For instance, the camera-face configuration, image resolution, and ambience lighting can impair facial feature extraction. Consequently, a facial image enhancement preprocessing step was implemented in the second portion of this work, significantly enhancing the precision of facial fatigue feature detection.

4.3.1 BF

In optimal non-fatigue, drivers blink rapidly due to external stimuli and objects. In an ideal mental state, blinking occurs at a rate of 15–20 times/min, each blink lasting 0.25–0.3 s.[19] Mild

fatigue reduces BF and extends blink interval; severe fatigue exhibits blinking near zero frequency and prolonged eye closure.

We scrutinized the test records of five drivers at 5-min intervals, as illustrated in Fig. 11. The visual examination indicates that as time progresses, BF variance diminishes gradually, although individual distinctions result in variation for some drivers compared with most individuals.

We isolated 10 specimens each from wakefulness, mild fatigue, fatigue, and severe fatigue via the acquired data and analyzed them using established methodologies. Different selection intervals were established; BF differences across fatigue stages were scrutinized, aiming to identify an optimal interval for fatigue parameter identification. Time segments of 30 and 60 s were selected to compute BF's mean and standard deviation sequentially. Analysis of variance is conducted to verify the distinction between these two under varying degrees of driver fatigue, as shown in Table 4.

From the data, there is notable variance in BF at $\alpha = 0.05$ significance level with a 30 or 60 s time window. Consequently, BF can serve as a fatigue indicator. To maximize fatigue detection, 60 s is chosen as the time window for BF.

4.3.2 PERCLOS

PERCLOS, a ratio of eyelid closure to time, indicates fatigue through demonstration of a positive correlation with its duration. We extracted real-time detection data from five test drivers, sampled at 5-min intervals. Results shown in Fig. 12 reveal that PERCLOS steadily increases over time, although personal variances cause minute deviations in PERCLOS values.

To evaluate the alterations in PERCLOS values with driver fatigue, 10 data points were randomly chosen for each fatigue state from a total pool of sample data. For 30 and 60 s time

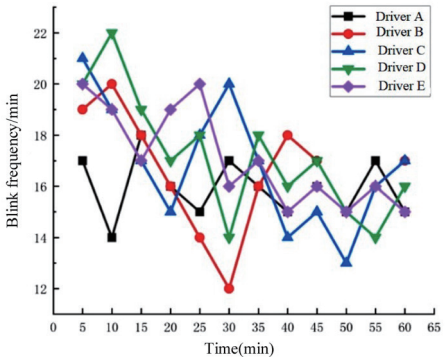

Fig. 11. (Color online) Driver BF

Table 4
Analysis of variance of driver's BF.

Parameters	Time window (s)	Awake		Mild fatigue		Fatigue		Severe fatigue		*F* value	*P* value
		Absolute mean	Standard deviation	Absolute mean	Standard deviation	Absolute mean	Standard deviation	Absolute mean	Standard deviation		
BF	30	15.105	3.891	15.301	3.880	13.750	4.013	12.532	4.336	8.512	0.035
	60	15.105	6.171	15.301	5.513	13.750	5.316	12.532	5.105	9.495	0.032

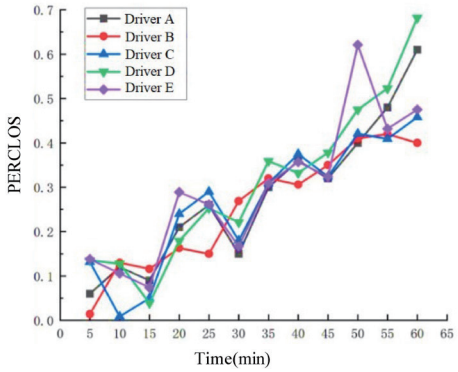

Fig. 12. (Color online) Driver's PERCLOS.

windows, the average and standard deviation of PERCLOS values were calculated and subjected to analysis of variance. The findings are tabulated in Table 5.

Evaluation of PERCLOS values within two selected time windows (30 and 60 s) indicated statistical significance at the $\alpha = 0.05$ threshold. Consequently, PERCLOS values serve as useful fatigue indicators. To simplify computations, we utilized a 30-s time frame for PERCLOS values.

4.3.3 Yawning frequency

Yawning serves as a physiological response of humans to combat fatigue. Fatigued individuals spontaneously yawn, relieving fatigue and transiently reinvigorating them.

In this study, we analyzed the empirical data of five test drivers, recording every 5 min, resulting in the yawning frequency curve shown in Fig. 13. This indicates that yawning frequency progressively increases with time, yet individual variances result in slight fluctuations.

5. Human–Machine Hybrid Enhanced Fatigue Monitoring Intelligent System

5.1 Back propagation (BP) neural network-based driver fatigue detection model

As shown in Fig. 14, in the BP neural network section, we configured the number of neurons in the input, output, and hidden layers, as well as the number of hidden layers. Subsequently, we selected the transfer functions and initial weight values for each layer. Lastly, we ascertained the learning efficacy and selected an appropriate expected error.

5.2 Input layer of BP

The driver fatigue driving detection model constructed in this study is based on the driver's driving state and facial features, and selects all fatigue feature parameters that satisfy significant differences in the third part as inputs to the model.

To mitigate the impact of dimensionality discrepancies across fatigue parameters and the transfer function's input-output amplitude, it is necessary to scale the model's input and output

Table 5
Analysis of variance of driver's PERCLOS.

Parameters	Time window (s)	Awake		Mild fatigue		Fatigue		Severe fatigue		*F* value	*P* value
		Absolute mean	Standard deviation	Absolute mean	Standard deviation	Absolute mean	Standard deviation	Absolute mean	Standard deviation		
PERCLOS	30	0.089	0.044	0.219	0.049	0.335	0.025	0.481	0.086	4.164	0.032
	60	0.088	0.040	0.225	0.041	0.346	0.026	0.535	0.082	3.231	0.043

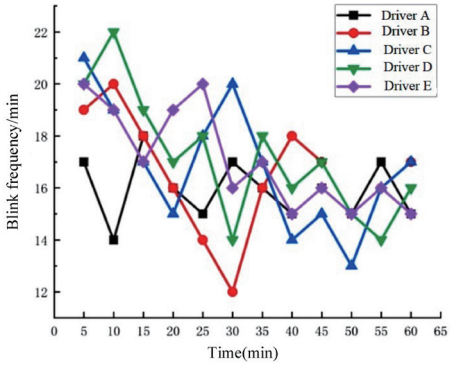

Fig. 13. (Color online) Driver BF.

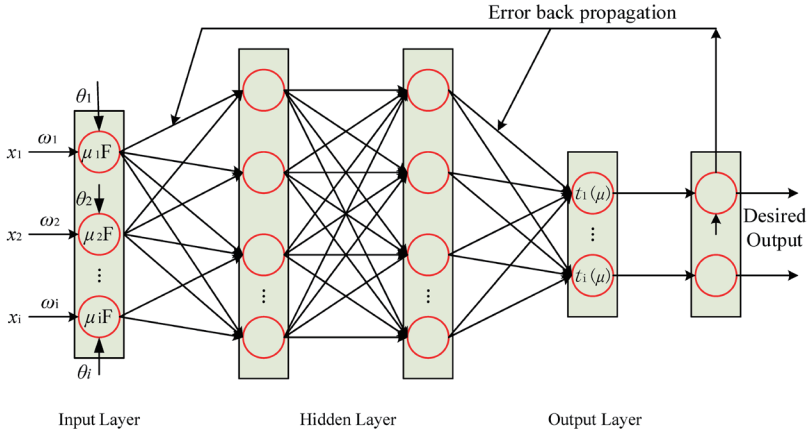

Fig. 14. (Color online) BP neural network-based driver fatigue detection model.

data to the interval [0,1] or [−1,1]. We employed the (0,1) normalization function within the Pycharm integrated ecosystem to standardize the input and output data.

5.3 Output layer of BP

The fatigue detection model constructed in this study is a four-level detection model, and the determined outputs are 1-awake, 2-mild fatigue, 3-fatigue, and 4-severe fatigue, with a quantity of 1. In this study, we used thresholds of 1.5, 2.5, and 3.5.

5.4 Hidden layer of BP

The model constructed in this paper includes only one hidden layer. We ultimately determined the number of hidden layer nodes to be 11.

As shown in Fig. 15, we proposed the BP neural net as the fusion algorithm for the driver fatigue detection model. Primarily, a state-of-the-art human–machine hybrid enhanced driver intelligent fatigue detection system was fashioned around a BP neural network-based driver fatigue detection model. Next, Python programming was utilized to formulate model programs

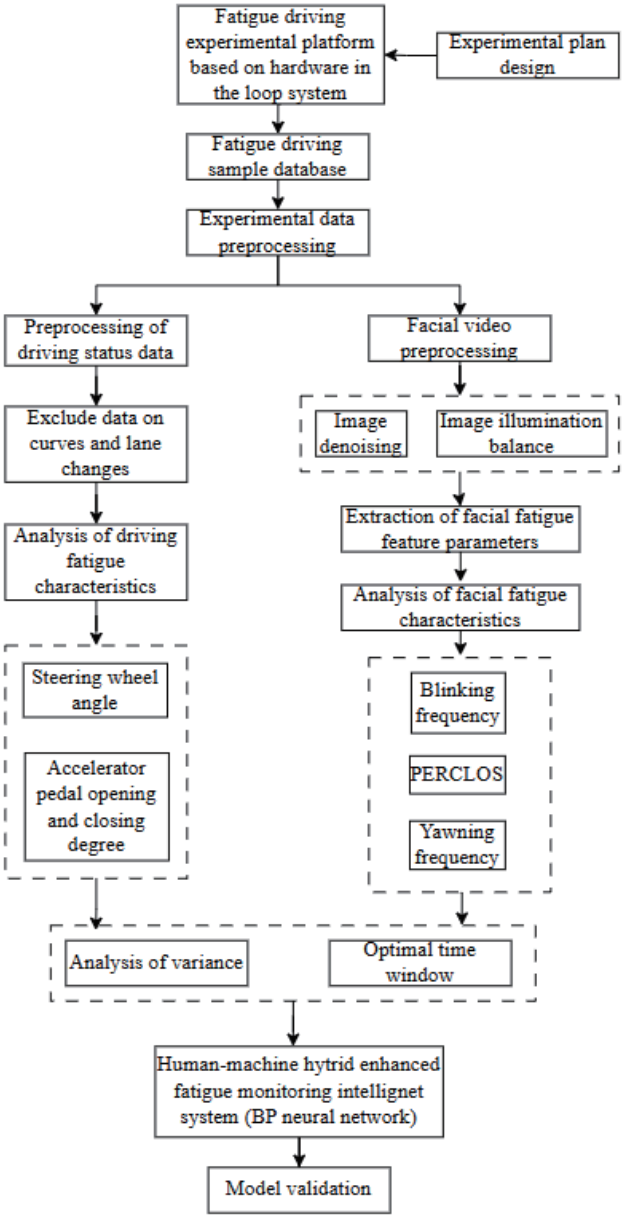

Fig. 15. Fatigue detection model based on human–machine hybrid enhanced intelligent system.

in the Pycharm environment. Lastly, an instance dataset was chosen at random from the established fatigue sample database for model training, validation, and testing. Refer to the diagram in Fig. 15 for the human–machine hybrid fatigue detection enhanced system.

The fatigue detection model based on the human–machine hybrid enhanced intelligent system devised in this paper constitutes a four-tier detection model, with the designated outcomes being 1-awake, 2-mild fatigue, 3-fatigue, and 4-severe fatigue.

6. Model Verification

Five hundred and sixty randomly selected sample data were procured from the fatigue driving sample database. This comprises 140 samples of wakefulness, mild fatigue, fatigue, and severe fatigue. One hundred and twenty samples from each fatigue level were designated as the requisite training data, and the remaining 20 sets constitute the test data. A Python-based script was devised for establishing a fatigue detection model using the Pycharm integrated development environment. The model was trained with samples representing different fatigue levels. To prevent overfitting, 480 sets of samples were divided into a 5:2:3 ratio for training, validation, and testing. The training and validation sets were utilized to refine the model, whereas the testing set was used to evaluate its performance. After iterative training, the error performance curve of the model is as shown in Figure 16.

Figure 16 shows the validation of the trained model through the analysis of error variations across different datasets. After 105 training instances, the model's mean square error tightened to 0.001, indicating an accelerated convergence rate due to the training data. It takes less time to achieve the expected mean square error. The remaining 80 samples comprise the validation set, with labels assigned as follows: label 1 = wakefulness, label 2 = mild fatigue, label 3 = fatigue, and label 4 = severe fatigue.

Figure 17 indicates the model's average accuracies of 95.5%, 91.5%, 94.7%, and 95.0% for differentiating four driver fatigue stages: wakefulness, mild fatigue, fatigue, and severe fatigue, respectively. This model is suitable for fatigue driving detection.

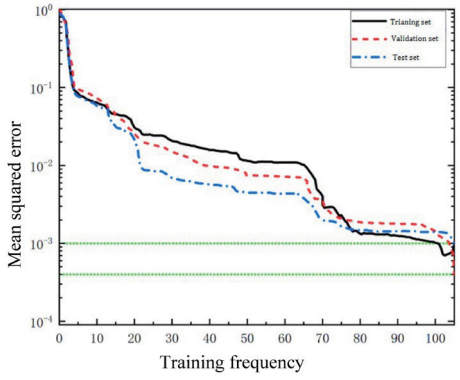

Fig. 16. (Color online) Detection model error performance curve.

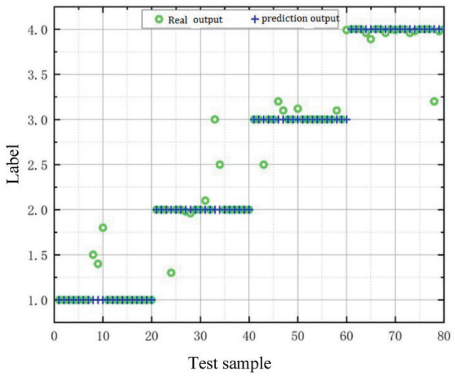

Fig. 17. (Color online) Verification results of fatigue detection model.

7. Conclusions

We developed a high-accuracy fatigue driving detection model using multi-feature fusion (combining driving state and facial features) and a BP neural network. Our main research results are as follows:

(1) A fatigue driving experimental platform was constructed by utilizing a six degree of freedom driving simulator, NI real-time machine, camera, and simulated driving simulation software (Carmaker, Matlab/Simulink). According to the designed experimental plan, a total of 9 drivers were invited to conduct experiments on two simulated roads: highways and urban expressways.

(2) The multi-feature fusion approach overcomes the limitations of single-source data, providing a stronger foundation for fatigue detection research.

(3) We built a fatigue detection model based on the BP neural network, and then used Python language to write the detection model program in the Pycharm integrated environment. The results showed that the model constructed in this paper had average accuracies of 95.5%, 91.5%, 94.7%, and 95.0% in detecting four levels of fatigue for drivers: wakefulness, mild fatigue, fatigue, and severe fatigue, respectively.

Acknowledgments

This work was supported in part by Special Projects in Key Fields of Colleges and Universities of Guangdong Province (New Generation Information Technology: 2021ZDZX1061 and 2023ZDZX1032), Characteristic Innovation Projects of Ordinary Colleges and Universities in Guangdong Province (2022KTSCX146), Zhaoqing University Youth Project (QN2024447), Zhaoqing Science and Technology Innovation Guidance Project (No. 241218114169466), and Innovative Research Team Project of Zhaoqing University (TD202423).

References

1 S. Houshmand, R. Kazemi, and H. Salmanzadeh: Proc. Inst. Mech. Eng. **235** (2021) 1069. https://doi.org/10.1177/09544119211017813
2 J. H. Jeong, B. W. Yu, D. H. Lee, and S. W. Lee: Brain Sci. **9** (2019) 2076. https://doi.org/10.3390/brainsci9120348
3 M. Gromer, D. Salb, T. Walzer, N. M. Madrid, and R. Seepold: Procedia Comput. Sci. **159** (2019) 1938. https://doi.org/10.1016/j.procs.2019.09.366
4 D. Gao, S. Liu, Y. Gao, P. Li, H. Zhang, M. Wang, S. Yan, L. Wang, and Y. Zhang: IEEE Trans. Fuzzy Syst. **33** (2025) 108. https://doi.org/10.1109/TFUZZ.2024.3399400
5 L. Zhong, M. Xu, J. Li, Z. Bai, H. Ji, L. Liu, and L. Jin: IEEE J. Biomed. Health. Inf. **29** (2025) 2603. https://doi.org/10.1093/eurjpc/zwaf236.514
6 Y. Guo, K. Yang, and Y. Wu: IEEE J. Biomed. Health. Inf. **29** (2025) 4009. https://doi.org/10.1109/JBHI.2025.3527964
7 F. Zhang, L. Dong, L. Zhang, X. Zhang, and X. Jiao: IEEE Trans. Intell. Transp. Syst. **23** (2025) 1. https://doi.org/10.1109/TITS.2025.3554808
8 D. F. Dinges and R. Grace: US Department of Transportation (1998) 112–113. https://doi.org/10.21949/1502740
9 C. Anitha, M. K. Venkatesha, and B. S. Adiga: Procedia Comput. Sci. **92** (2016) 63. https://doi.org/10.1016/j.procs.2016.07.324

10 T. Zhu , C. Zhang, T. Wu, Z. Ouyang, H. Li, X. Na, J. Liang, and W. Li: Appl Sci. **12** (2022) 2224. https://doi.org/10.3390/app12042224
11 A. D. McDonald, J. D. Lee, and C. Schwarz: Accid Anal Prev. **13** (2020) 25. https://doi.org/10.1016/j.aap.2018.01.005
12 Z. Li, L. Chen, L. Nie, and S. X. Yang: IEEE Tvt. **71** (2021) 269. https://doi.org/10.1109/TVT.2021.3130152
13 R. Li, Y. V. Chen, and L. Zhang: Int J Ind Ergonom. **82** (2021) 103083. https://doi.org/10.1016/j.ergon.2021.103083
14 J. Zhu, Q. Liu, Z. Zhao, Y. Lu, Z. Yao, and Q. Li: IEEE Trans. Intell. Transp. Syst. **23** (2025) 13. https://doi.org/10.1109/TITS.2025.3550818
15 D. Pomerleau: Proc.1995 Intelligent Vehicles Symposium Conf. (IEEE,1995) 25–26.
16 S. X. Cai, C. K. Du, S. Y. Zhou, and Y. F. Wang: Trans Sys Eng and Infor Tech. **20** (2020) 77. http://www.tseit.org.cn/CN/Y2020/V20/I4/77
17 P. Getreuer: Image Processing. **20** (2012) 266. https://doi.org/10.5201/ipol.2012.g-ace
18 P. M. Narendra and R. C. Fitch: IEEE Trans. Pattern Anal. Mach. Intell. **6** (1981) 655. https://doi.org/10.1109/TPAMI.1981.4767166
19 V. Kazemi and J. Sullivan: Proc. 2014 IEEE computer vision and pattern recognition Conf. (2014) 3–5.